Pin–Hole Luminosity Monitor with Feedback*

JAMES H. NOREM[†]

Argonne National Laboratory, 9700 South Cass Ave.

Argonne, Illinois, 60439, USA

JAMES E. SPENCER[‡]

Accelerator Research Department B, Stanford Linear Accelerator Center, 2575 Sand Hill Rd.

Menlo Park, California, 94025, USA

Previously, the generalized luminosity $\mathcal{L}$ was defined and calculated for all incident channels based on an NLC e^+e^- design. Alternatives were then considered to improve the differing beam-beam effects in the e^-e^-, $e\gamma$ and $\gamma\gamma$ channels. Regardless of the channel, there was a large flux of outgoing, high energy photons that were produced from the beam-beam interaction e.g. beamsstrahlung that needs to be disposed of and whose flux depended on $\mathcal{L}$. One approach to this problem is to consider it a resource and attempt to take advantage of it by disposing of these straight–ahead photons in more useful ways than simply dumping them. While there are many options for monitoring the luminosity, any method that allows feedback and optimization in real time and in a non-intercepting and non-interfering way during normal data taking is extremely important – especially if it provides other capabilities such as high resolution tuning of spot sizes and can be used for all incident channels without essential modifications to their setup. Our "pin-hole" camera appears to be such a device if it can be made to work with high energy photons in ways that are compatible with the many other constraints and demands on space around the interaction region. The basis for using this method is that it has, in principle, the inherent resolution and bandwidth to monitor the very small spot sizes and their stabilities that are required for very high, integrated luminosity. While there are many possible, simultaneous uses of these outgoing photon beams, we limit our discussion to a single, blind, proof-of-principle experiment that was done on the FFTB line at SLAC to certify the concept of a camera obscura for high energy photons.

Keywords: lasers; damage; luminosity; pin–hole camera; camera obscura; brightness; figure–of–merit; transmissive, reflective modes.

1. General Introduction and Background

Recently, an interesting controversy has arisen in the art world concerning the use of such a technique by early Renaissance artists[?]. This is an ongoing debate that has attracted the attention of physicists but with differing conclusions. Regardless of where one stands on the subject, it is intriguing because it involves so many diverse disciplines, historical implications and concepts such as "originality".
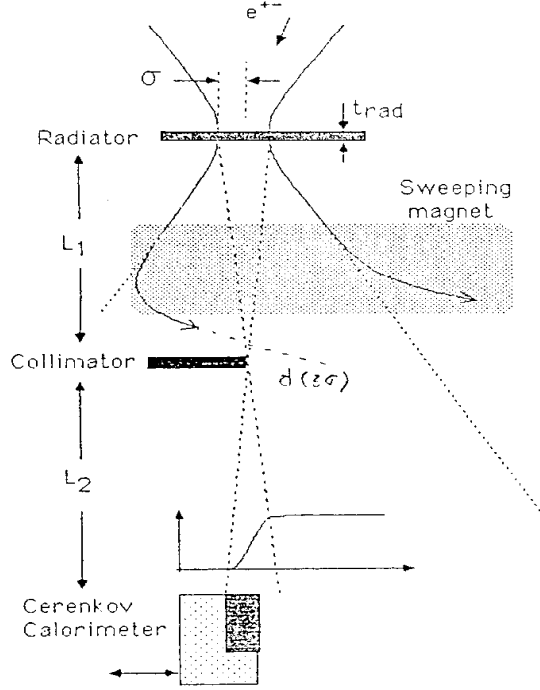

Fig. 1.   Simplified, schematic view of a possible pin-hole camera arrangement for a variety of uses.

For the present authors, the key point in the technique involves the luminosity required for the method to work effectively rather than whether any famous names actually used it[?]. In conventional terms, the pinhole camera requires a great deal of light or source illumination and/or a very good light gathering lens or system. In modern terms one calls it is a very slow camera implying a very large f-stop but this can be missleading.

Figure 1 gives a stylized example that shows the basics for implementing such a device for use with higher energy photons than light or x–rays. In the figure, a beam impinges at the top on some form of radiator having an effective thickness t_{rad} consistent with the beam energy and the material. This is followed by a sweeping magnet that provides at least 3σ distance from the beam at the collimator (pin–hole) located at L_1 downstream to avoid any unnecessary background from this collimator. Typically, neither the radiator nor this magnet would be necessary in an NLC setup but they are shown here because they relate to the FFTB experiment. The collimator is followed by a detector at L_2. For $L_2 = L_1$, the magnification is 1:1 with the profile given by the derivative which can be effected in several ways e.g. if the dark area associated with the detector is taken to be the right side of the upper collimator or pin–hole then we can scan this to get a profile or simply open it by moving to the right to capture the whole profile with a position sensitive detector such as a ccd.

We note that the image is inverted here but if you were a renaissance painter using this method then you could also have used a silver salver (from your wealthy

patron) to reflect the image whose upright size would depend on the magnification L_2/L_1 which, in its turn, is constrained by your available light intensity.

1.1. *Applications*

There are many but we mention only those based on Figs. 1–2. The conceptual layout in Fig. 1 is relevant for the Final Focus Test Beam (FFTB) at SLAC because the experiment (E152) began as a bremsstrahlung monitor for the FFTB spot size. Later, we decided that it also could be a good monitor for the Compton backscattered photons produced at IP1 for the Nonlinear QED Experiment E144 in the dump line of the FFTB. In particular, it could monitor both the laser–electron overlap at IP1 as well as the efficiency of the conversion process that is especially relevant for the $\gamma\gamma$ channel of a General Linear Collider (GLC) where the laser intensity implies serious multiple scattering effects.

In the present example, we show how this could be relevant for an FFTB final focus beam or for setup of the beams for an NLC. Thus, in Fig. 2, we suppose that we're checking or tuning the chromaticity correction at the FF or possibly the bunch–to–bunch energy jitter. By taking a sequence of single bunch shots with no unintentional changes to the upstream beam line we can minimize the spot size via the slope or derivative of the profile at the detector/slit in Figs. 1 and 2. Likewise, if we take multiple shots when intensity is a problem or the strength of an effect is weak, we can monitor the stability from the spread which could be a good way to study bunch-to-bunch or head-tail wake effects based on charge jitter.

Having begun the paper with an historical perspective, we followed with a basic
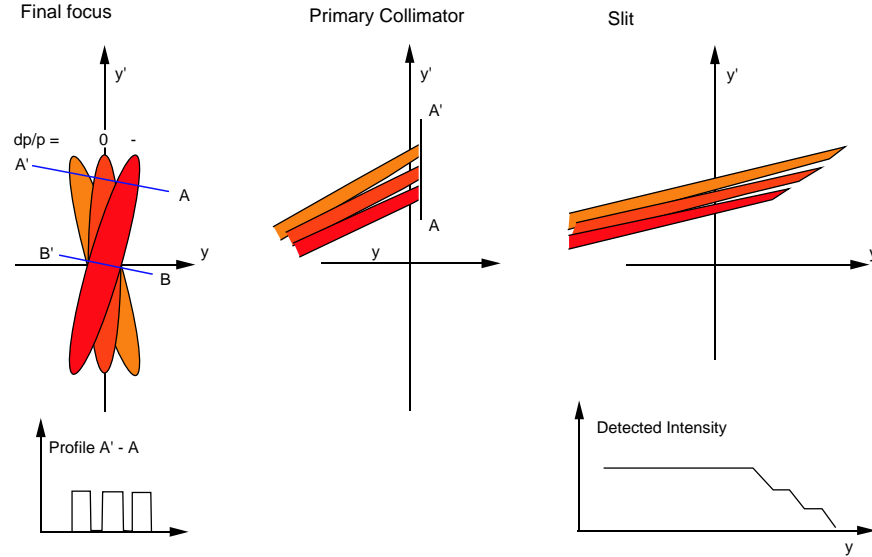

Fig. 2. Schematic of how to use Fig. 1 to tune chromaticity or monitor momentum stability.

description applicable to a number of applications and then described how and why such a setup could be useful in ways that are not necessarily apparent for a pin–hole beyond observing solar eclipses[?] due to their high intensities. Next, before giving a description of the FFTB experiment and some results from it we first discuss the luminosity to show that the high energy γ intensity is so strong that it allows several, simultaneous possibilities but seems ideal for some variant of the pin–hole camera technique. In closing, we note that this experiment was done in 1997 but we are only discussing it now because it is both timely and interesting — if not as interesting as the art world controversy.

2. Figures-of-Merit

2.1. *Luminosity*

The most important figure-of-merit for colliders is the total, integrated, usable luminosity. The generalized luminosity[?,?] was based on the observation that **all** colliding beam machines as well as **all** incident channels in any particular GLC can be expected to have a luminosity proportional to the square of the *primary*, incident bunch 'charge' (N_B^2 or $n_B N_B^2$ or $n_x n_y n_z N_B^2$ or $n_z (n_x n_y N_B)^2$) that can be brought into collision per unit time within an effective area that contains the *effective* number $\widehat{N}_B$ based on conversion efficiencies and detector constraints[?,?,?]. For a laser driven accelerator, where the laser and electron normalized emittances are matched, one can write, in terms of the standard NLC expression

$$\mathcal{L} \;=\; \frac{f_T n_B N_B^2 H_D}{4\pi \sigma_x^* \sigma_y^*} \zeta \equiv \mathcal{L}_{\mathrm{G}} H_D \zeta \;\rightarrow\; \frac{f_T n_B N_B^2 \gamma H_D}{4\pi \epsilon_n \beta^*} \;\zeta \;\propto\; \frac{P_b}{\lambda Z_R} N_B H_D \zeta \qquad (1)$$

where the various parameters are the usual ones[?,?,?] e.g. $\sigma_{x,y}^*$ is the undisrupted, rms spot size at the interaction point and β^* is the magneto-optical 'depth-of-field' at the IP. The arrow simplifies to round beams and $P_b \propto f n N E_b$ is the incident, primary electron beam power. β^* is equivalent to the Rayleigh range $Z_R > \lambda$, the laser wavelength. In this scenario, luminosity increases with decreasing λ^2. Table I gives the results for NLC e^+e^- configurations[?] at $\mathrm{E_{cm}}{=}500$ and 1000 GeV as well as when they are run with e^-e^- together with corresponding results for an e^-e^- configuration called "Santa Cruz"[?] that was developed for another e^-e^- meeting.

Notice that the e^-e^- results for each configuration is given in the lower box set off by double lines while the e^+e^- results are in the upper boxes e.g. in the first column we see that there are 0.98 outgoing γs per incident electron in the e^+e^- channel but 0.95 when the configuration uses e^-e^-. The average energy of these γs is $0.033\mathrm{E_\circ}$ and $0.32\mathrm{E_\circ}$ respectively or $\langle \mathrm{E}_\gamma \rangle \approx 8.25$ GeV. Similarly, the fate of these photons parses into different outgoing channels e.g. there are effective $e\gamma$ and $\gamma\gamma$ channels having $\mathcal{L}_{Compton}$ and $\mathcal{L}_{\gamma\gamma}$ of 0.23 and 0.10 in units of $[10^{34}\mathrm{m}^{-2}\mathrm{sec}^{-1}]$ in the e^+e^- channel:

$$\mathcal{R} \;=\; (\mathcal{L}_{Compton} + \mathcal{L}_{\gamma\gamma})/\mathcal{L}_{ee} = 0.55 \;. \qquad (2)$$

For the e^+e^- channel in the 500SC configuration, the corresponding value is 0.69 which is worse by the ratio 1.26 but in the e^-e^- incident channel, the corresponding

Table I: Beam–Beam effects for e^+e^- and e^-e^- at E_{cm}=500 and 1000 GeV. Basic NLC configurations have an 'A' while (...) are analytic calculations rather than simulations.

$\sqrt{s}_{NLC}$ [GeV]	500A	500SC	1000A	1000SC
f_{rep}[Hz]	180		120	
n_B	90		90	
$N_B[10^9]$	6.5	0.80	9.5	0.80
$P_B/E_B \equiv n_B N_B f_{rep}[10^{12}]$	105.3	105.3	102.6	102.6
$\gamma\epsilon_x/\gamma\epsilon_y$ $[10^{-8}m]$	500/8	8/8	500/10	10/10
σ_x^*/σ_y^*[nm]	285.9/4.52	36.2/4.52	226.1/3.57	32.0/3.57
$\sigma_z[\mu m]$	100	100	125	125
β_x^*/β_y^*[mm]	8/0.125	8/0.125	10/0.125	10/0.125
$\mathcal{L}_G[10^{34}\text{m}^{-2}\text{sec}^{-1}]$	0.42	0.41	0.96	0.57
$|D_x|/|D_y|$	(0.090/5.70)	(0.626/5.01)	(0.132/8.33)	(0.507/4.53)
θ_D [μrad]	(257)	(226)	(238)	(130)
Υ	(0.10)	(0.09)	(0.30)	(0.18)
$H_D \equiv \mathcal{L}_{e\pm}/\mathcal{L}_G$	1.42	2.02	1.36	1.67
$\mathcal{L}_{e\pm}[10^{34}\text{m}^{-2}\text{sec}^{-1}]$	0.60	0.85	1.30	0.95
$\langle s\rangle/s_{NLC}$	0.972	0.941	0.913	0.922
s_{rms}/s_{NLC}	0.068	0.106	0.144	0.137
$\langle E_\circ - E_{in}\rangle/E_{in}$	0.032	0.054	0.103	0.073
$\delta_B \equiv (E_\circ)_{rms}/E_{in}$	0.065	0.097	0.142	0.121
$\mathcal{L}_{100}/\mathcal{L}_{e\pm}$	0.376	0.299	0.195	0.287
N_γ/N_e	0.98	1.29	1.67	1.30
$\langle E_\gamma\rangle/E_\circ$	0.033	0.042	0.062	0.056
$\mathcal{L}_{Compton}$	0.23	0.41	0.80	0.45
$\mathcal{L}_{\gamma\gamma}[10^{34}\text{m}^{-2}\text{sec}^{-1}]$	0.10	0.18	0.56	0.35
$H_D \equiv \mathcal{L}/\mathcal{L}_G$	0.55	0.52	0.47	0.54
$\mathcal{L}_{e^-e^-}[10^{34}\text{m}^{-2}\text{sec}^{-1}]$	0.23	0.21	0.45	0.31
$\langle s\rangle/s_{NLC}$	0.980	0.985	0.940	0.97
$\langle E_\circ - E_{in}\rangle/E_{in}$	0.031	0.025	0.095	0.041
$\delta_B \equiv (E_\circ)_{rms}/E_{in}$	0.064	0.056	0.138	0.084
$\mathcal{L}_{100}/\mathcal{L}_{e\pm}$	0.396	0.449	0.215	0.408
N_γ/N_e	0.95	0.83	1.60	0.93
$\langle E_\gamma\rangle/E_\circ$	0.032	0.031	0.059	0.045

number inverts to ∼0.87 – the relative number of outgoing photons in the two cases. Clearly, the e^+e^- results are better for the 500A configuration while 500SC is better for e^-e^-. No modifications were assumed necessary here beyond certain magnetic polarity reversals so they are mechanically the same. There was no attempt to basically redesign the line to simultaneously optimize both $\mathcal{R}$ and $\mathcal{L}_{ee}$ in a way that comprehends different configurations but based on the same mechanical layout. The degree to which this is possible and acceptable should then suggest some heuristic changes that breaks their mechanical similarity but in easily modifiable ways.

2.2. *Brightness and other measures and constraints*

While $\mathcal{L}$ and the impedances associated with the accelerator are important, we know that there are many subsystems with their own FoMs and one of the most important concepts where misunderstanding occurs relates directly to the beam itself. Liouville's theorem and the Vlasov equation, in varying approximations, place good lower bounds on what is ultimately achievable and is why one places so much importance on the source. Clearly, every bunch or bunchlet determines the instantaneous luminosity but also the outgoing γ phase space. For bremsstrahlung from 46 GeV electrons, the conversion process adds essentially nothing to the transverse emittances because the spot size doesn't change appreciably from the effective wire size if $\sigma >$ d, the wire diameter but it can become somewhat distorted whereas the angular divergence remains essentially unchanged for stable beams. The longitudinal emittance does change however so this needs consideration depending on the application. Here it enters in our choice of the converter thickness that is also used to filter the lower energy photon flux.

While there are far more questions than we can answer here, it is important to note that the only meaningful statement for the distribution function in terms of the canonical variables in six dimensional phase space is that the *local* density is an invariant. This assumes noninteracting particles even though the electrons collide and interact through collective space charge and self magnetic fields whose influence varies with energy. However, the former are negligible compared with the smoothed fields of the latter when the Debye length is 'large' i.e. $n\lambda_D^3 \gg 1$ or the number of particles in a Debye sphere is large. This is often the case and will be assumed. For photons, the equivalent is the photon wavelength.

This is especially true for the frequencies implied for laser driven accelerators where both the microbunch lengths and transverse emittances should all be a fraction ($\approx \frac{\lambda}{4\pi}$) of the optical wavelength. While this apparently argues in favor of longer wavelength lasers, the problem is significant for any laser wavelength and therefore implies that new techniques are needed before any of the new high-gradient, high-frequency acceleration schemes that are currently under consideration become feasible.

The quantity that best represents the fully invariant 6D phase space for linear, time independent systems is the normalized brightness whether we're interested in particle or photon beams of any kind:

$$B_n^6 \;=\; \frac{N_B}{\epsilon_{nx}\epsilon_{ny}\sigma_z\sigma_\gamma} \tag{3}$$

where N_B stands for the number of quasiparticles in a "bunch" and σ_z and σ_γ are the bunchlet's rms length and energy spread. For photons, σ_γ, the normalized energy spread in units of mc^2, could be taken simply as σ_ω and σ_z as σ_t giving B_n^6 as a photon density:

$$B_n^6 \;=\; (4\pi)^2 \frac{N_B}{\lambda^2 \sigma_t \sigma_\omega/\overline{\omega}}\eta \leq 10^{16}\eta/\lambda^3 \;. \tag{4}$$

η is a conversion efficiency e.g. of electrons to photons so that it is a function of several variables but certainly ω and depending on the conversion process e.g. bremsstrahlung, Compton or beam-beam as well as any subsequent filtering process.

3. The FFTB Experiment

Figure 3 shows the FFTB dump line layout that was used for this experiment. There are now three collimators called C1 nearest the source at IP1 and two down-stream collimators: USlit or S1 and LSlit or S2. The distances that are shown were determined partly by the fact that all of these were mounted in what is called the gamma line or the straight-ahead line after the permanent magnet (PM) dump line magnets that bend the ≤10 kW electron beam into the ground after the FF and IP1 locations in the FFTB. All collimators had 200 μm gage blocks separating the top and bottom halves of optically ground tungsten surfaces of $\sim$3.5 inch thick absorber blocks that could be positioned to better than one μm.

We were given one eight hour shift of beam beginning at midnight on May 24. Almost immediately, the beam went off for several hours. Recovering the beam and starting from a different experiment, we tuned the FFTB to give a flat beam of approximate size $\sigma_x=\sigma_y\approx$1 mm on an AlO fluorescent screen ($\sim$20 mils thick) at IP1 downstream of the FF that we used to roughly align the slits on the bremsstrahlung γ beam while getting it through to our detector. On the same actuator as the AlO screen there was an unknown combination of wires that could be inserted. A 1 mm sigma should allow us to see all wires without too much loss of intensity because we had been told only that there were ≤3 horizontal wires separated by approximately 1 mm stretched across an opening of unknown vertical size in an Aluminum frame (16 mil Al foil). We were not told the wire sizes or their materials or even whether they were the same size or material but we did have some knowledge of the wire inventory.

By 5:30 AM we had obtained a reasonably stable beam and found and centered

Fig. 3.   Schematic elevation view of the pin–hole camera experiment in the FFTB dump line.
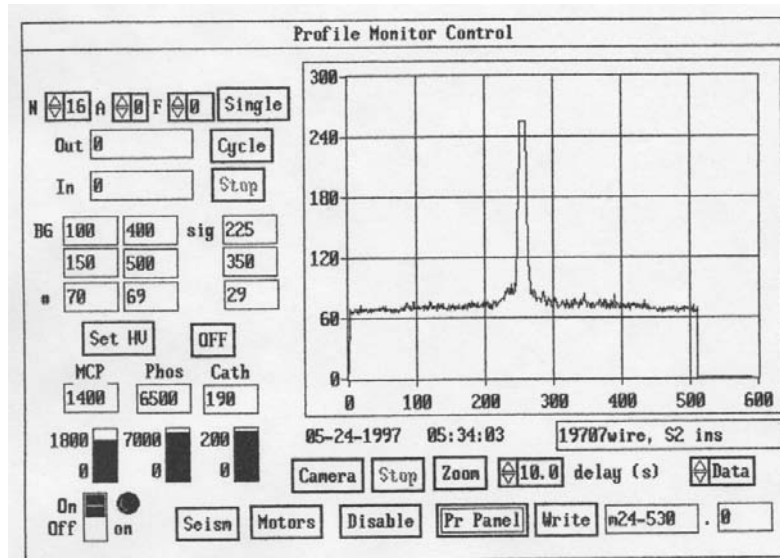
Fig. 4.   Typical control panel view for data from this run showing a CCD profile based on Fig. 3.

the profile shown on the control panel layout in Fig 4. This shows the output of the CCD in Fig. 3 with a single, strong peak obtained with the collimator C1 effectively pulled out as was S1 but with the S2 or LSlit in so that we were roughly aligned on the beam and observing it from one or more wires the 512 channel CCD. This was the start of the data sequence M24-530.0 taken at 5:34 AM. The different blocks in the figure lead to other panels e.g. the "Motors" block goes to a panel that sets and reads the absolute and relative positions in height of each slit, the step size for
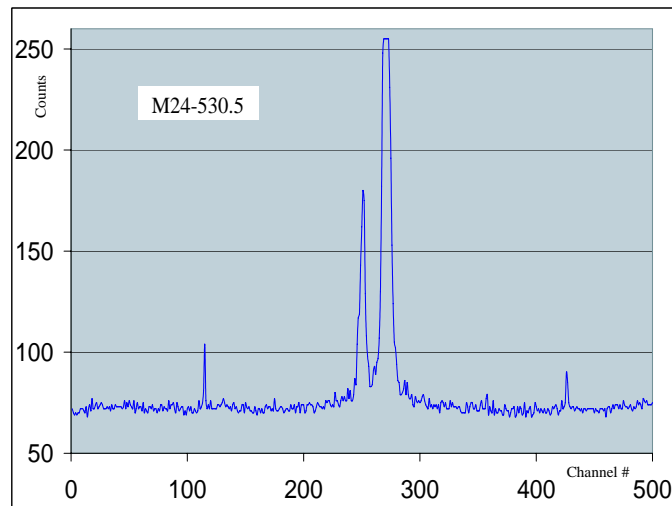
Fig. 5.   Early data from the CCD output showing profiles of two wires and the frame edges.
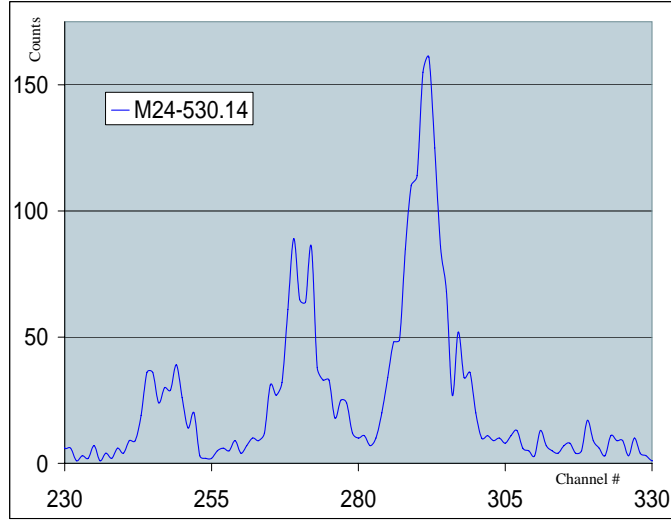
Fig. 6.   Run 14 data showing profiles for three wires but with unstable beam conditions.

any move as well as the pitch and roll of each slit that has a three prong support. Run 5 of the M24-530 sequence was taken at 6:13 AM and is shown in Fig. 5 using an EXCEL spreadsheet plot.

The wire frame was left unmoved initially because it determined the vertical beam position at the wire but with S2 pulled out i.e repositioned somewhat to improve the count rate which was reduced when C1 was run inwards and the pitch varied to better define the beam and improve the magnification. Notice that the strongest peak in both Figs. 4–5 is strongly saturated at 255 counts from the 8-bit ADC which proved to be a major limitation.
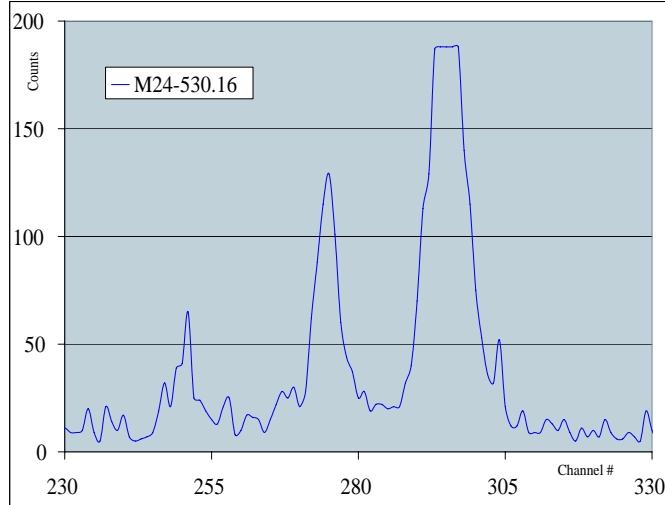
Fig. 7.   Run 16 data showing profiles for three wires with improved beam conditions.
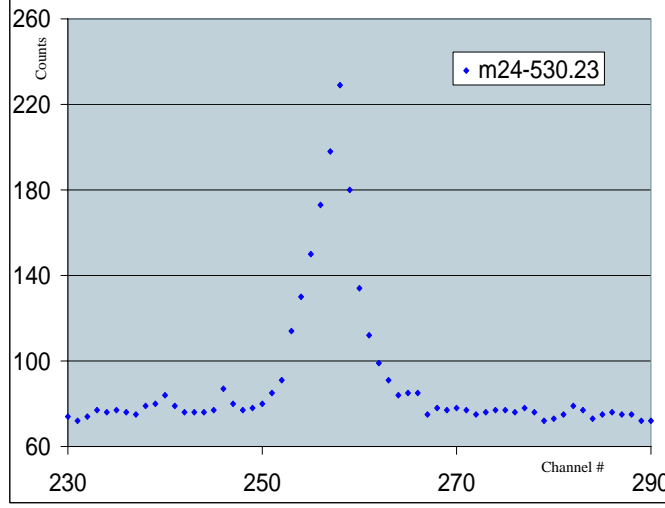
Fig. 8.   Run 23 data showing a profile for one wire with all collimators partially in.

Figure 6 shows another run in the sequence taken at 7:08 AM showing three wires but with unstable beam conditions - presumably related to RF problems leading to energy fluctuations or any effect that leads to an angle change at the wires. This profile was obtained after scanning the wire frame vertically and increasing the MCP voltage. We were able to keep three wires visible for a scanning range of more than 300 μm. In this plot we did a constant background subtraction. There appears to be at least four discrete peaks per wire profile here where two are stronger and two weaker with the weaker ones at the sides so that there may have been some beam clipping for these. Three wires are fully resolved and have a mean separation starting from the lowest of ∼24.5 and 21 pixels respectively. Assuming similar materials, this implies that the wire sizes go in the ratio of 1:2.3:4.1.

Figure 7 shows another run in the sequence taken at 7:12 AM showing three wires but with more stable beam so their separations are better resolved being ∼25 and 20 pixels respectively. Again, the integrated counts go in the ratio of 1:2.4:4.9 even though the upper peak has five saturated pixels. Although the wire frame was not moved between these runs there is a clear shift in position that can explain the differences in ratios between Run 14 and 16. Under these conditions, at this time in the morning, one expects such things so we decided to start closing the slits to measure individual profile widths, one at a time, by scanning the wire frame to position each succeeding wire to place its images at the same location on the focal plane.

Figure 8 shows an example of this — Run 23 that was taken at 7:40 AM. This program was not completed before we lost beam at ∼8 AM. There is no evidence for other wires on either side of the single peak but it seems clear that there are still additional peaks especially on the low side but we can't fit this to get a unique wire σ_y. Given more time, the program would have been to reduce integration times by
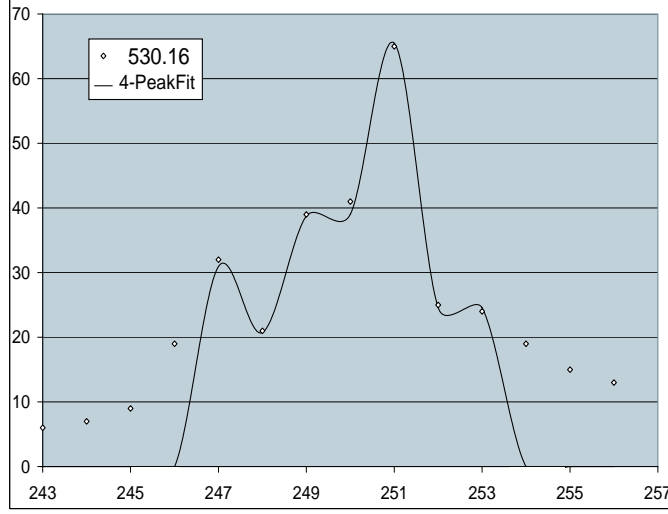
Fig. 9. Run 16 data showing a 4-peak gaussian fit to the profile for the lowest wire in Fig. 7.

increasing voltage on the MCP, sequentially optimizing the height, pitch and roll of the collimators as well as increasingly strong vertical focussing at the wires. The radiation length[?] goes as:

$$L_{rad} \; = \; \frac{716.4A}{Z(Z+1)ln(287/\sqrt{Z})} \quad \left[\frac{\text{g}}{\text{cm}^2}\right] \; .$$ (5)

The mean thickness of a circular wire of diameter d is d/π and the rms thickness spread is $d/2\sqrt{2}$. Some possible materials include C_{12}^6, Al_{27}^{13}, and W_{184}^{74} in various diameters up to 34 μm with radiation lengths of 18.8, 8.9 and 0.35 cm, respectively. Taking the ratio of the mean thickness of a d μm wire with L_{rad} one gets a normalized, relative thickness of 1:2.1:53.7.

Clearly, one prefers Tungsten for the smallest diameter. However, if we assume that all wires were of the same unspecified material then the simplest interpretation from Figs. 6 and 7 is $\sim$5, 10 and 20 μm based on what we know of the available wire sizes. To help certify this possibility, we fit the different peaks — especially the lower ones which are and should be better defined than the stronger ones in terms of their components, if indeed, they come from thinner wires and thus should be resolved better. Also, these runs provide an absolute definition of pixel size and therefore wire size in contrast to Fig. 8.

Fitting the lowest group in Fig. 7 near channel #250 with 4 peaks spanning $\sim$8 pixels gave a good fit with a common gaussian rms width of 0.15 pixels as shown in Fig. 9. Assuming an average separation of the wires of 22.5 px implies $\sim$45 μm per pixel and a wire size d=19 μm. From our choice of wires, this must be a 20 μm Al wire and the stronger peaks in the higher channels were then the 5 and 10 μm W. This is, in fact, what we were told had been installed. Furthermore, the wire separations of $\sim$25 and 20 pixels had been measured to be 1.18 and 0.94 mm respectively giving a ratio of 1.255 corresponding to our measurement of 1.25. Further, a

consistent measure of the wire frame's vertical aperture was ≤1.5 cm.

4. Concluding Remarks

All of the results presented above were obtained during a single 8 hour shift with considerably less than 8 hours of beam time. While we did not prove our conclusions from this blind-test due to lack of time and stable running conditions that necessitated shortcuts, we believe that we demonstrated what we set out to accomplish. Clearly, the worst mistake or shortcoming was in using an 8-bit ADC. Also, one would like an absolute way to calibrate the pixel spacing i.e. the magnification or, at least, a good relative measure without requiring two or more wires. Figure 10 shows some serious improvements over the setup used in the current experiment where a streak camera is used instead of the CCD and ADC. This is based on the expected intensity of the beamsstrahlung and could allow a measurement of the individual bunch densities i in a train $\rho_i(y(z))$. Relevant to the overall application of the method, this figure shows the conventional pin–hole at the top-left and the collimator or half pin–hole where the measured intensity at y is:

$$\mathrm{I}(y) \;=\; \int_0^y I(y)|_{y'\sim 0} dy \tag{6}$$

showing the derivative relation. We note that the intrinsic resolution of this method based on the oscillations of the penumbra from the collimator is the geometric mean of the photon wavelength and the distance b in Fig. 10 or L_1 in Fig. 1 i.e. 16 m in our case shown in Fig. 3. Assuming a mean energy of 8 GeV for the beamsstrahlung from an E_{cm}=500 GeV collider given in Table I, which is also reasonable for the present experiment, gives $\delta=\sqrt{L\lambda/2}$=25 nm. Clearly, increasing L worsens the resolution so some natural feature that allows a small, removable half collimator could be useful at times. Nevertheless, very high resolution and very high repetition rates are often mutually exclusive but this is not the case here so that some variant of this method in conjunction with others and the beam disposal problem should be considered.

Acknowledgements

References

1. David Hockney, *Secret Knowledge: Rediscovering the Lost Techniques of the Old Masters.*, (Viking, New York, 2001). Also: Philip Steadman, *Vermeer's Camera*, Oxford, London, 2001.

2. Aristotle was aware of the principle and Alhazen used it some eight hundred years ago to view solar eclipses which is still its most universal use today. Similarly, Leonardo da Vinci's (1452–1519) notebooks contain several descriptions of this first camera but it assumed its modern form only after a photosensitive recording medium was placed near the image plane. However, if Leonardo did not use it for painting, it would be a pity because then he would have used it to make one of the first, permanent, recording mediums i.e. a camera in the modern sense. He was the ideal of the renaissance person who some claim ushered in this period and others claim was the first scientist in modern terms based on his use of mathematics to inform both his art and perspective. In his day, the method must have seemed like magic but like all good science, it begins in wonder and scepticism and ends in the commonplace but there is almost always something new to be learned when one looks a little closer. Insofar as Leonardo is concerned, there is no doubt that his use of this technique could help to explain his prodigious overall output as well as to justify the artist/scientist rubric but, for his sake, one wishes that it was true if for no other reason than the joy he would have experienced to have painted the Mona Lisa informed with this additional perspective eye to study his subject.

3. J.E. Spencer, Beam-Beam Effects and Generalized Luminosity, *Intl. J. Mod. Phys.* **11** (1996) 1675.

4. J.E. Spencer, Limitations Imposed by Beam-Beam Effects and Their Remedies, *Intl. J. Mod. Phys.* **13** (1998) 2479.

5. J.E. Spencer, Limitations Imposed by Beam-Beam Effects and Their Remedies - II, *Intl. J. Mod. Phys.* **15** (2000) 2543.

6. Zeroth-Order Design Report for the Next Linear Collider, May 1996, SLAC Report 474, LBNL-PUB-5424, UCRL-ID-124161.

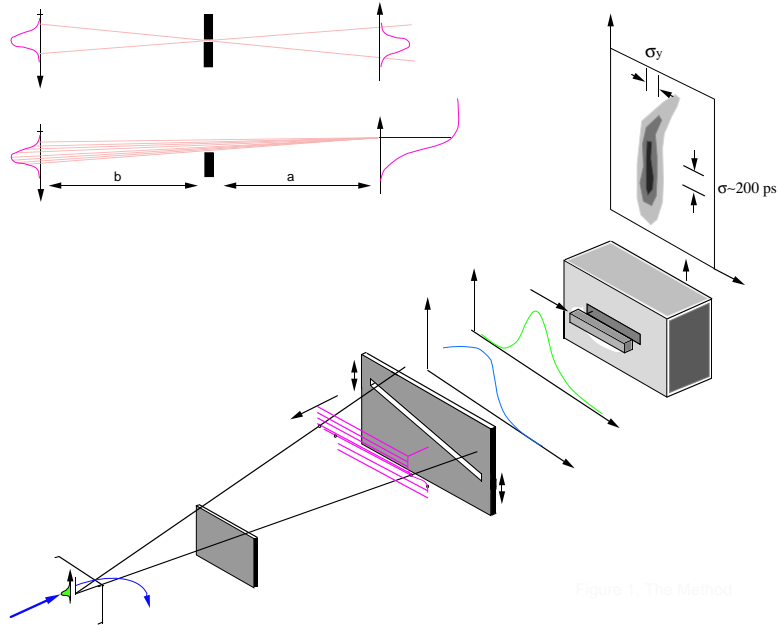7. European Physical Journal C, **Vol. 15** (2000) 1-878.

Fig. 10. More general schematic of an improved pin–hole camera with faster recording medium applicable for use with a bremsstrahlung radiator, Compton converter or collider beamsstrahlung.